

Investigation of geophysical anomalies in soil depth and assessment of salt irrigation impact on soil quality at Ain El Atti experimental station, south-eastern of Morocco

Ahmed Hamidi^{1*} , Ibrahim Dakir² , Ahmed Benamara¹ ,
Lhoussine Tarik³ , Ibrahim Salhi¹ 

¹ Department of Mechanical and Structures Engineering, National Graduate School of Arts and Crafts, Moulay Ismail University, Marjane 2, B.P. 15290 Al-Mansor, Meknes, Morocco

² Laboratory of Marine Geosciences and Soil Sciences, Department of Geology, Faculty of Sciences, Chouaib Edoukkali University, Avenue Jabran Khalil Jabran, B.P. 299-24000, El Jadida, Morocco

³ Department of Geosciences, Faculty of Sciences and Techniques, Moulay Ismail University, Boutalamine, BP 509, Errachidia, Morocco

* Corresponding author's e-mail: ahmedhamidi642@gmail.com

ABSTRACT

Soil salinity in the southern region of Errachidia represents a major environmental challenge, particularly in arid environments where freshwater resources are scarce. This study aims to characterize the interactions between local lithology and experimental agricultural practices to assess the impact of saline irrigation on soil quality. Advanced geophysical methods, combining very low frequency electromagnetic (VLF-EM) and electrical resistivity tomography (ERT), were applied at the Ain El Atti experimental site to map geological structures and analyze the distribution of salinity. The results revealed a highly conductive and relatively homogeneous subsurface. A NW-SE oriented fracture anomaly (with current density varying between 4 and 10%) in the SW part of the study area, identified through three-dimensional analysis, plays a key role in groundwater drainage and circulation, thereby influencing the spatial distribution of salinity. The resistivity pseudo-sections confirmed these findings, showing slightly resistive values ($> 100 \Omega \cdot m$) at depths of 10–15 meters, associated with alluvial and conglomeratic deposits. In contrast, deeper horizons exhibited high conductivity, attributed to marls and water-saturated sands, indicating significant salinity levels. These results, influenced by hydrogeological variability and irrigation practices, highlight the need for complementary hydrochemical and hydrogeological analyses. Nevertheless, this study provides crucial insights for soil and water management in arid regions. Identifying drainage structures could help optimize irrigation strategies and reduce soil degradation. The combined VLF-EM and ERT approach enhances the understanding of salinization processes and offers valuable perspectives for similar studies in other environmental contexts.

Keywords: Ain El Atti experimental station, soil salinity, electrical resistivity tomography, VLF-electromagnetic method.

INTRODUCTION

The Errachidia-Tafilalet region is located in the southern part of the Eastern High Atlas. It faces significant challenges, including water scarcity and poor water quality, due to the prolonged droughts it has experienced in recent decades (Ammary, 2007). Agriculture represents 90% of the local economy and is directly linked

to the availability of wadis, springs, and khetarras, which have been used by the local population since ancient times.

To optimize the use of saline water in arid areas, the National Institute of Agronomic Research (INRA) has conducted soil tests by experimenting with plant species. This experiment aimed not only at economic objectives, such as increasing agricultural yield and production, but also

at reducing the impact of desertification in the region. It is therefore for environmental reasons that the researchers conducted this study, which aims to examine the ability of these plant species to grow and adapt to irrigation with saline water from the deep aquifer (Ammary, 2007).

Electromagnetic measurements play a key role in geophysical exploration, providing detailed information on the vertical and lateral distribution of conductive structures. These structures may indicate the presence of groundwater or mineralized zones. The very low frequency (VLF) electromagnetic method is widely used in hydrogeophysical and environmental prospecting, allowing the identification of high-conductivity areas associated with groundwater flow, mineralized fractures, and soils subjected to salinization (Ammar & Kruse, 2016; Ait Bahammou et al., 2019; Dakir et al., 2021). The electrical resistivity method, and more specifically ERT, has been widely applied in many exploration projects (Chiara et al., 2019; Horo et al., 2020; Olenchenko & Osipova, 2022). It has also been extensively used in environmental studies (Dakir et al., 2020; Ait Bahammou et al., 2021; Chidiebere et al., 2023).

This study is conducted at the Ain El Atti experimental site, covering a land area of approximately 10 hectares. It adopts a combined approach using two distinct geophysical methods for hydrogeophysical exploration. VLF-EM data will be analyzed to establish a detailed map

of lithological and structural units (Benson et al., 1997). These results will then be compared and validated using data obtained from ERT. The interpretation of the electrical data will allow for the delineation of geophysical anomalies at depth and the evaluation, both vertically and horizontally, of the impact of saline irrigation on soil quality. This approach will also help highlight the heterogeneity of the studied area.

GEOGRAPHICAL AND GEOLOGICAL SETTING

The study area is located approximately 45 km southeast of the city of Errachidia and 14 km northeast of Erfoud. It belongs to the topographic map of Errachidia at a scale of 1:100,000. Access to the area is via the N13 national road, which connects Errachidia to Erfoud, up to kilometeric point 58 from Errachidia, located near the study area (Figure 1). From a geological perspective, the area is located between two major structural domains of Morocco: the High Atlas to the north and the Anti-Atlas to the south, more specifically within the Cretaceous Errachidia Basin. This basin is presented as a dissymmetrical synclinoorium, consisting of Cenomanian-Turonian carbonate deposits, gravelly-sandy formations with intercalations of gypsum from the Infracenomanian, as well as clayey sands containing evaporite

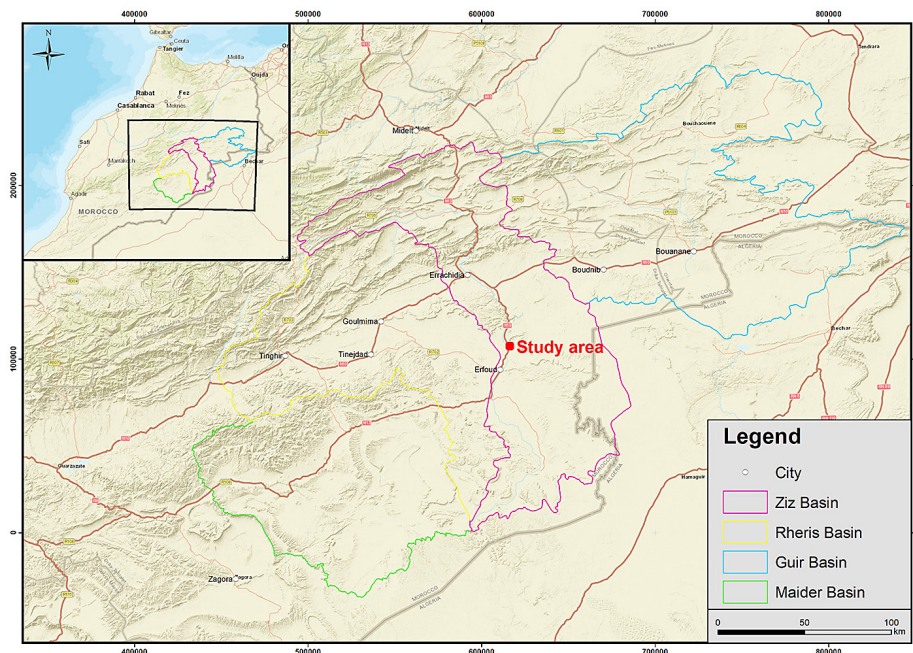


Figure 1. Geographical location of the study area

deposits and gypsiferous formations from the Senonian (Figure 2).

The Infracenomanian is primarily composed of red marls, continental-origin sandstones, white marls, and red clays containing gypsum layers (Choubert, 1920–1945) (Figure 3). After the Albian regression, the Cenomanian-Turonian formations consist of limestone beds resting directly on the red clays with gypsum. At the top of the Cretaceous

series, fine detrital deposits cover the Turonian limestones (Choubert & Faure-Muret, 1962).

HYDROGEOLOGICAL DATA

The low rainfall in the Errachidia-Boudnib Basin limits surface water recharge, making the region heavily reliant on groundwater resources

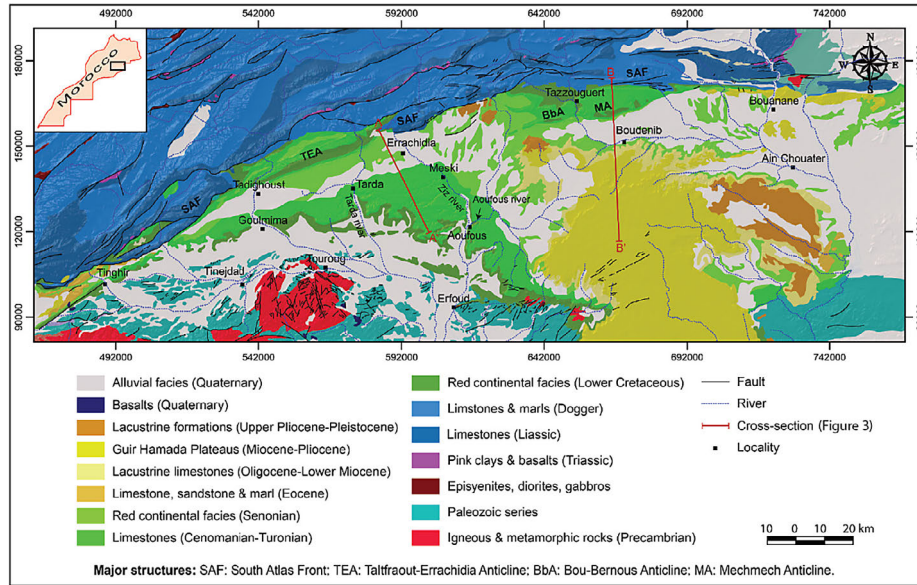


Figure 2. Geological map of the Errachidia basin, adapted from the geological map of Morocco (1:1 000 000) by Hollard et al., (1985) and modified by Bouzekraoui et al., (2023)

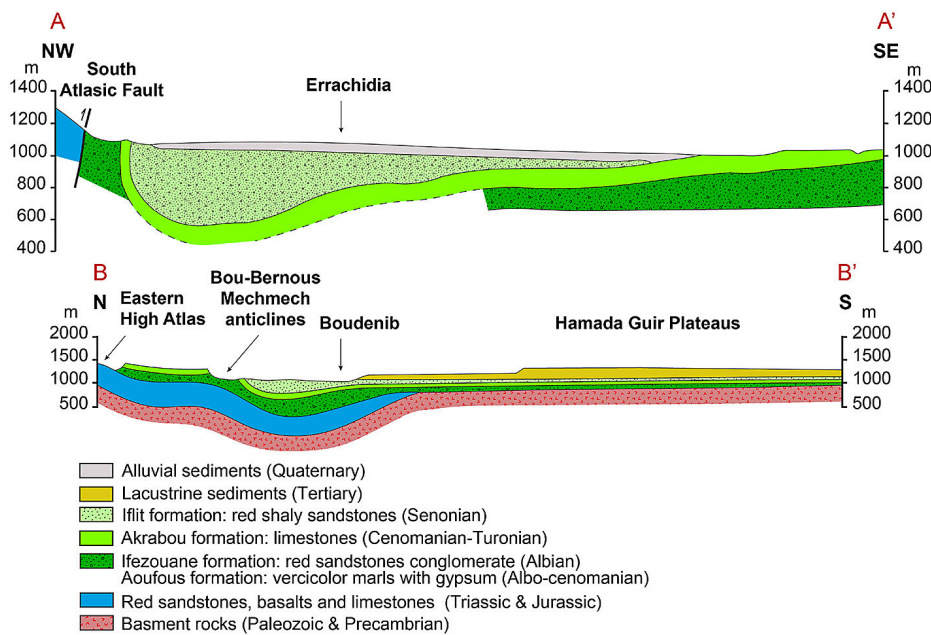


Figure 3. Geological cross-sections (A-A' and B-B') illustrating the regional asymmetrical structure of the Errachidia basin, Adapted from Chamayou & Ruhard, (1977), and Revised by Bouzekraoui et al., (2023) (for location, see Fig. 2)

and hydraulic infrastructure. The hydrographic network is mainly dominated by the Ziz River, which originates in the High Atlas and flows from north to south, providing drainage and water supply to the downstream areas. To optimize the management of this resource and support local agriculture, the Hassan-Dakhil Dam was built on the Ziz River. This dam regulates the flow, stores water during flood periods, and ensures controlled distribution for irrigating agricultural lands downstream. In addition to its agricultural role, the dam also helps provide drinking water and offers protection against occasional, though rare, flooding. However, the dominance of the arid climate and prolonged droughts increase the challenges associated with sustainable water resource management in the region (Figure 4).

In the Cretaceous Errachidia Basin, groundwater is a crucial resource due to the scarcity of precipitation and limited surface water contribution. The basin is divided into two main types of aquifers: shallow aquifers, mainly found along the valleys, and deep aquifers, which are essential for the region’s water supply (Figure 5). This basin consists of a multi-layered aquifer system with four primary aquifer levels (Margat, 1977).

The Infracenomanian artesian aquifer is composed of continental deposits (coarse sandstones and conglomerates) and lagoonal formations (sands, clays, and marls). The Turonian aquifer consists of fractured limestone formations and marine dolomites, often in karstic facies. The Senonian aquifer is made up of highly heterogeneous continental sandstone-clay formations containing gypsum and anhydrite (Ammary, 2007). Lastly, the Quaternary aquifer, located in the southern part of the basin and corresponding to the Tafilalet aquifer, rests on a base of more or less cemented conglomerates and lacustrine sandstones, forming the primary water reserve for this aquifer (Margat, 1977). From a hydrogeological standpoint, these deep aquifers are structured into three major units running from north to south: the High Atlas, where aquifers are linked to fractured and carbonated formations; the Cretaceous Errachidia Basin, where aquifers develop within Cretaceous sedimentary formations that alternate between permeable and impermeable levels; and the Anti-Atlas, where aquifers are often associated with older formations and tectonic structures that affect their recharge and circulation (Ammary, 2007).

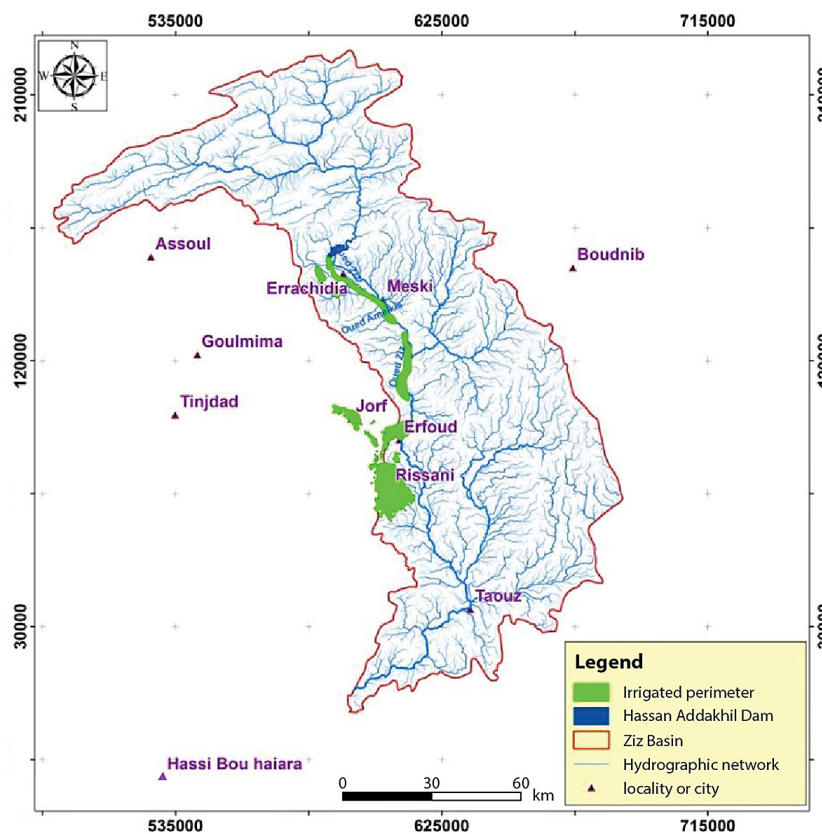


Figure 4. Map of the irrigated area of the Tafilalet Plain (Ben-said et al., 2017)

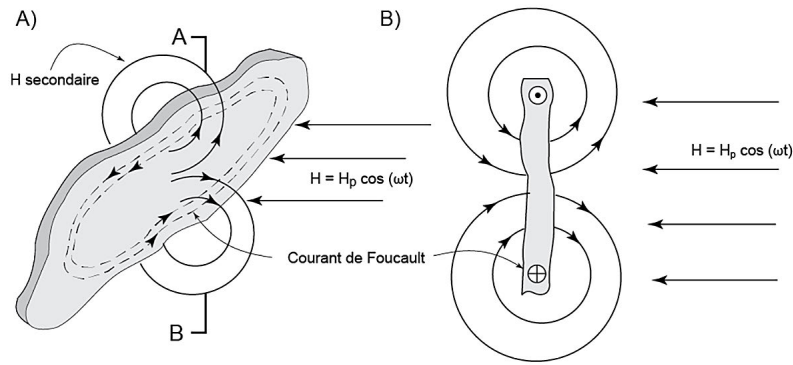


Figure 6. Electromagnetic induction: Perspective view (a) and cross-section along A-B (b) (Chouteau, 2001)

$$f_{2-3} = (M3 + M4) - (M1 + M2) \quad (3)$$

where: $M1$ to $M4$ – represent four successive points along the profile, and the result is plotted between points $M2$ and $M3$.

Applying the Fraser filter to tilt data (real component) generates peak values as positive spikes, thereby revealing the presence of a conductive structure (Sungkono, 2017).

Karous-Hjelt filter

Karous and Hjelt (1983) developed a filtering technique known as the Karous–Hjelt (K–H) filter. It is an extension of the Fraser filter, based on Biot–Savart’s law and applied to the real component of the apparent current density at a given depth. The magnetic field is generated by a current source, and a linear filter was developed to calculate the current density using Biot–Savart’s law (Gürer et al., 2009; Sharma et al., 2014; Kumar et al., 2020). A 2D pseudo-section is then constructed based on variations in current density with depth (Sharma et al., 2014). High current density zones indicate the presence of conductive structures, while low-density zones correspond to resistive media (Tarik et al., 2023) (Equation 4).

$$\frac{\Delta z}{2\pi} I_{\alpha}(0) = -0.102H_{-3} + 0.059H_{-2} - 0.561H_{-1} + 0.561H_1 - 0.059H_2 - 0.102H_3 \quad (4)$$

where: $I_{\alpha}(0) = 0.5 \left[I \left(\frac{\Delta x}{2} \right) + I \left(-\frac{\Delta x}{2} \right) \right]$ – equivalent to the current density, and I is the current. Δz - depth at which the current density is calculated, with a data interval of Δz .

Euler deconvolution

Euler deconvolution (Thompson, 1982) is one of the most commonly used semi-automated

methods for depth estimation in VLF-EM interpretations (Ebrahimi et al., 2019). It enables source localization without requiring prior assumptions about its physical properties (Pašteka & Kušnirák, 2020). The 3D Euler deconvolution Equation 5 (Thompson, 1982; Reid et al., 1990) can be expressed as follows:

$$(x - x_0) \frac{\partial IP}{\partial x} + (y - y_0) \frac{\partial IP}{\partial y} + (z - z_0) \frac{\partial IP}{\partial z} = N(IP' - IP) \quad (5)$$

where: x_0 , y_0 and z_0 – corresponds to causative source; IP' – back ground field, while IP – denotes the Fraser-filtered in-phase anomaly measured at points x , y , z . N – structural index (SI), which characterizes the geometry of the source.

The SI is defined as the rate of change of the anomaly with depth. It helps determine the shape of the body (Reid et al., 1990; Thompson, 1982; Reid et al., 2014). The derived Euler deconvolution (DED) method applies Euler deconvolution to the sum of the vertical and horizontal derivatives of the data. These data are first filtered using the Fraser filter to improve accuracy. In this case, the structural index (SI) is increased by 1 (Cooper, 2004; Tarik et al., 2023).

Geoelectrical surveys

The classical method of ERT relies on measuring the electrical resistivity of the subsurface. Resistivity data were collected along 14 profiles, each 320 meters long and oriented SW-NE, using the ABEM Terrameter LS equipment from Georeva (Figure 7). In this study, the Wenner configuration in tomography was chosen for its high signal intensity, its ability to provide high resolution of

horizontal structures, and its excellent signal-to-noise ratio (Loke, 2004; Seaton & Burbey, 2002; Sharma & Verma, 2015).

The nominal electrode spacing “a” for each dipole was set at 5 meters. Measurements were taken in Tomography or Electrical Panel mode using a set of 64 non-polarizable electrodes connected by 4 multi-conductor cables. The Lambert North coordinate system, with the Merchich datum, was used for mapping the terrain via ERT and for geo-referencing the profile lines. Data inversion was performed using the Res2Dinv software from Geotomo Software (Loke & Barker, 1996a).

The following Equation 6 defines the apparent resistivity ρ_a at each measurement point:

$$\rho_a = K \cdot \frac{\Delta V}{I} \quad (6)$$

where: ΔV – potential difference, I – injected current intensity, and $K = 2\pi a$ is the geometric factor that depends on the setup used.

RESULTS AND DISCUSSION

The results of the Karous-Hjelt filter, Fraser filter and Euler deconvolution

Figure 8 presents a series of pseudo-sections obtained by applying the Karous-Hjelt filter to the VLF-EM data for six profiles (L1 to L6). The goal of this filter is to transform the surface-measured data into a vertical section, providing an

approximate idea of the depth of conductive structures. These pseudo-sections highlight conductor axes marked by a high electrical current density, indicating structures that enhance electrical conductivity. These axes show a dip to the southwest (SW) and predominantly appear between 500 and 800 meters on profiles L1, L3, L4, L5, and L6. The most pronounced anomalies are located at depths between -40 and -60 meters, with varying intensity depending on the profiles. Profiles L4 and L6 exhibit the strongest anomalies, suggesting a high concentration of conductive chemical elements, possibly from saline irrigation or capillary rise of salinity through identified fractures. In contrast, profiles L2 and L5 show greater homogeneity, which may indicate an area less affected by the circulation of mineralized water. The orientation and continuity of the conductor axes suggest the presence of a NW-SE-oriented fracture network, likely facilitating the infiltration and migration of mineralized fluids. This fracture anomaly could thus play a key role in groundwater recharge from the High Atlas.

Figure 9 presents the map of the Fraser filter applied to the tilt angle of the secondary magnetic field. This filter aims to enhance the resolution of conductive anomalies and better visualize the transition zones between materials of different conductivities. Examining the Fraser map suggests the presence of six anomalies (A1 to A6), which are elongated and rounded, with amplitudes ranging from 1% to 5.4%. Anomaly A1,

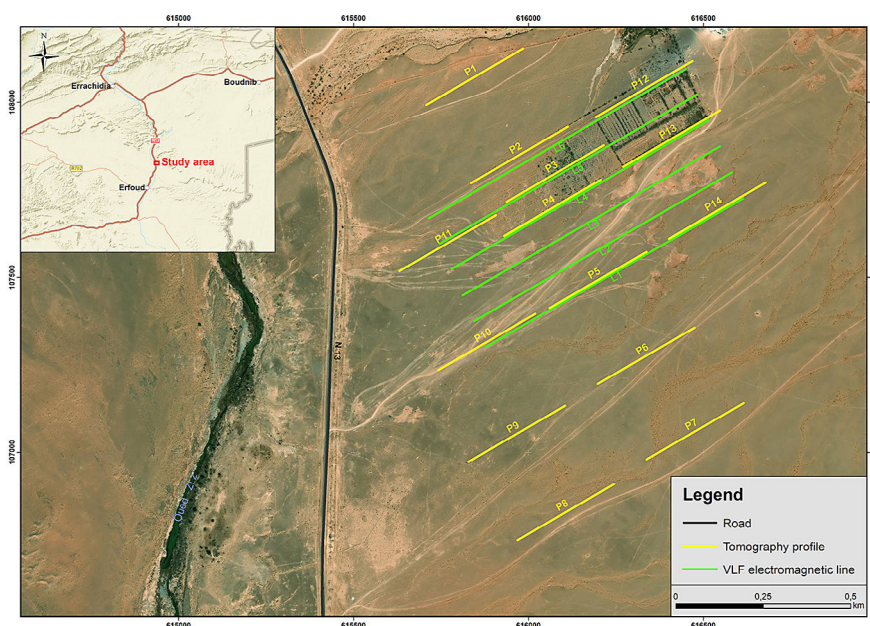


Figure 7. Location of the electrical tomography profiles and EM-VLF lines conducted in the study area

oriented NW-SE, is well-identified in the southwest part of the area, while anomalies A2, A3, and A4, cylindrical in shape, are located in the central part of the area, specifically in the irrigated plots. These conductive anomalies are attributed to areas of salinity accumulation, resulting from both saline irrigation and capillary rise of salinity from deeper levels. The map also identifies two other

anomalies, A5 and A6, located in the eastern part of the surveyed area. These anomalies, aligned in a NW-SE direction, are attributed to the passage of a fault that facilitates the flow of water from the High Atlas.

The characterization of deep structures requires an advanced data processing approach, integrating a quantitative analysis of the magnetic

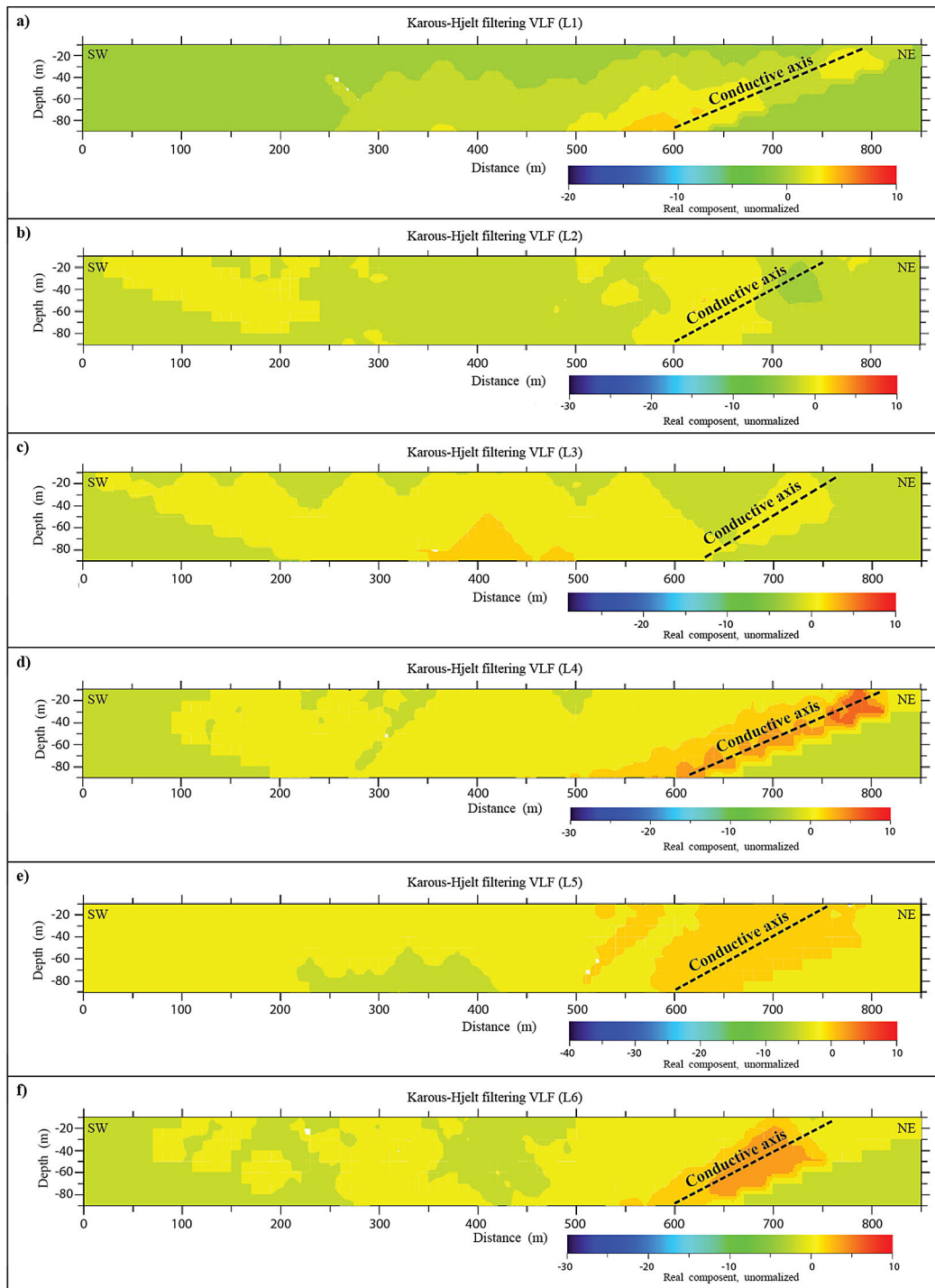


Figure 8. Pseudo-sections of the data filtered by the Karous-Hjelt method for the 6 VLF-EM profiles (spacing = 10 m)

component of the electromagnetic measurements. This approach allows inferring essential subsurface parameters, such as geological structures, contacts, and the depth of bodies responsible for the anomalies. In this study, we applied the Euler deconvolution transformation to the data from the Fraser filter, using a structural index $SI = 1$, to delineate geological bodies and contacts, and estimate their depths. For magnetic data analysis, several researchers (Thompson, 1982; Reid et al., 1990) have demonstrated that the structural index (N) varies from 0 to 3 depending on the structures considered: $N = 0$ for contacts and faults with significant displacement, $N = 1$ for faults with minor displacement and dykes, $N = 2$ for a cylindrical structure, and $N = 3$ for a spherical structure. Figure 10 presents the Euler solutions superimposed on the Fraser filter map, with depths ranging from 0 to > 80 meters. These values, represented by colored circles, indicate the position of magnetic sources. Blue represents depths from 0 to 30 m, yellow from 31 to 45 m, green from 45 to 80 m, and red for depths greater than 80 m. Overall, the blue, yellow, and green circles dominate,

suggesting that the average depth of the magnetic sources lies between the surface and 80 m. This distribution indicates the presence of few deep structures, particularly at the A3 anomaly, where the salinity concentration results from irrigation. Finally, the analysis of the Euler solutions reveals that most of the magnetized structures are aligned in a preferred NW-SE direction, highlighting a structural organization consistent with regional tectonic processes.

Processing of electrical resistivity tomography (ERT) data

To confirm the results obtained by the low-frequency electromagnetic method (VLF-EM), assess the influence of salinity on the study area, and analyze the characteristic heterogeneities of the experimental station of Ain El Atti in comparison with its surroundings, we measured the subsurface resistivity. For this purpose, 14 electrical profiles were carried out using ERT method. All the profiles (Figure 11) reveal significant variations in apparent resistivity, reflecting

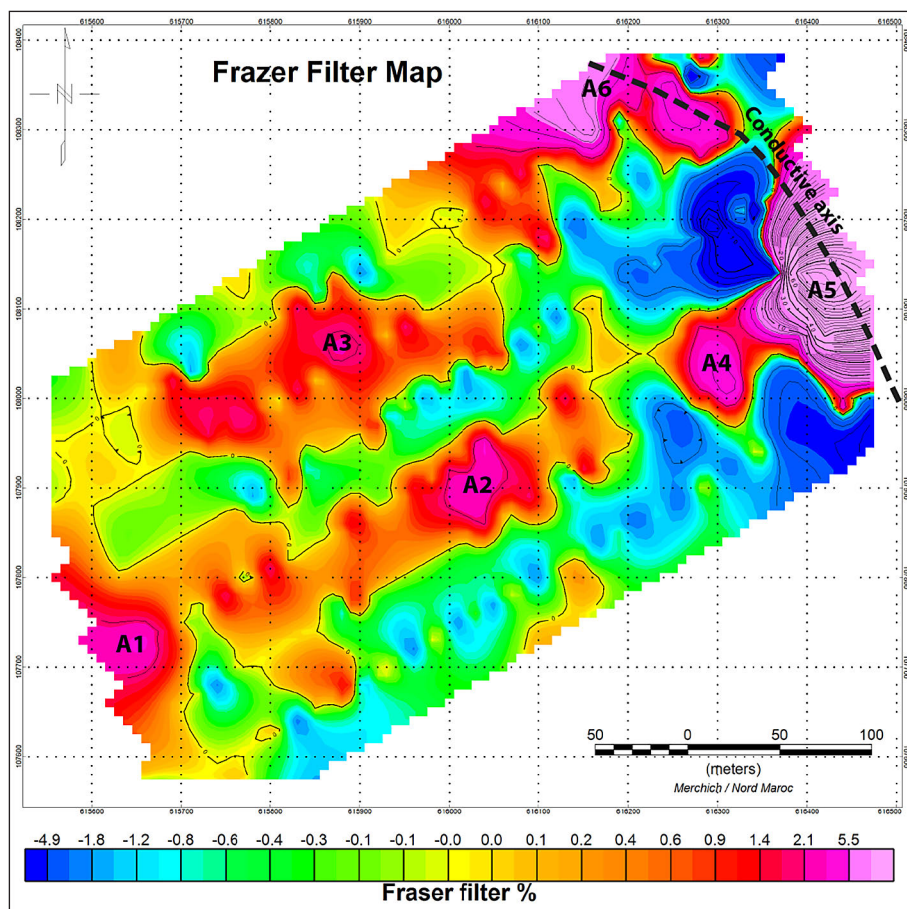


Figure 9. Map of the real component filtered by the Fraser filter

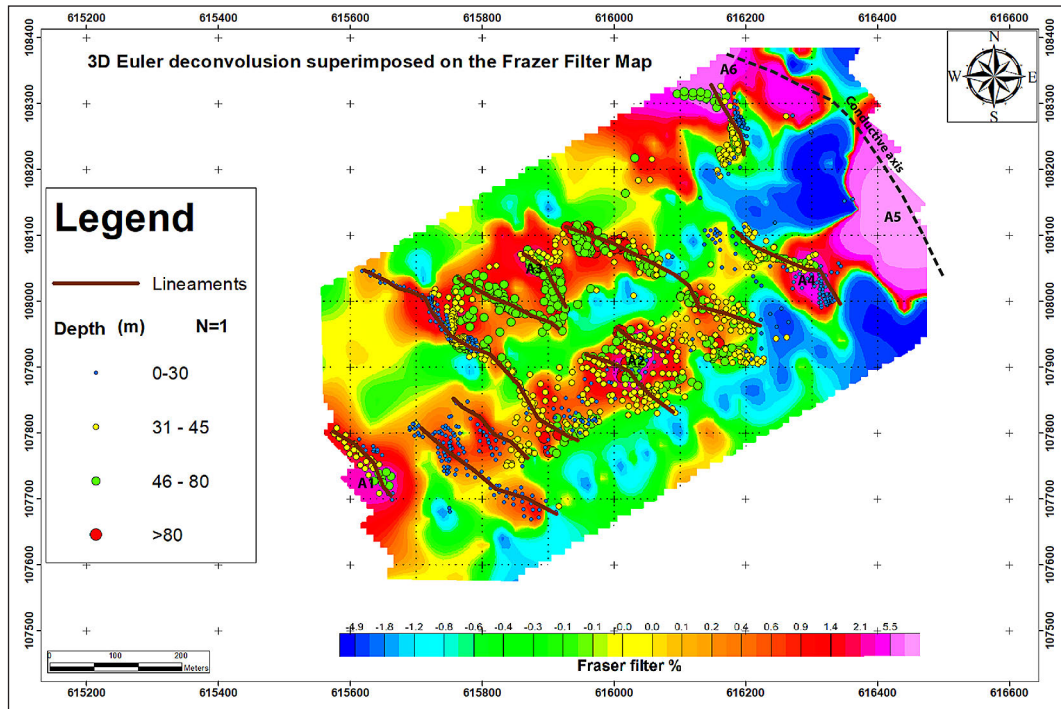


Figure 10. 3D Euler solutions for the study area with a structural index (N) and a maximum relative tolerance of 1 and 15%, respectively, with a window grid size of 10×10 m

the geological complexity of the studied subsurface. All models show that the resistivity is very high at the surface, while it becomes conductive from 5 meters deep. Profile 1 (Figure 11a), conducted outside the experimental site of Ain El Atti, shows low resistivity at depth (5 to 10 $\Omega \cdot m$), attributed to marly and sandy formations from the infracenomanian age. At the surface, resistivity is high (100 to 120 $\Omega \cdot m$) due to the presence of in-situ conglomerates associated with a concretion process linked to saline irrigation. Profiles 2, 3, and 4 (Figures 11b, 11c, and 11d) were conducted within the experimental station. The formations crossed by these profiles have a sub-tabular structure and show resistivity variations both laterally at the surface and vertically at depth. In the northeast part of the profiles, saline irrigation has led to a decrease in the resistivity of the surface layers (40 to 50 $\Omega \cdot m$), while increasing their thickness. In contrast, at the beginning of the profiles, where soil disturbance is absent, the surface resistivity is higher (80 to 100 $\Omega \cdot m$). At depth, resistivity remains low (5 to 10 $\Omega \cdot m$). Profiles 5, 6, and 7 (Figures 11e, 11f, and 11g) were conducted to the south of the experimental site, following the same NE-SW direction. They show similarities with the first profile taken to the north of the station. The upper part of the profiles is characterized by high resistivity,

especially at the beginning of the trace (80 to 100 $\Omega \cdot m$). In the center and east of the profiles, resistivity is moderate (30 to 50 $\Omega \cdot m$), a variation attributable to the composition of the surface layer, which may consist of silt, alluvium, or Quaternary conglomerates. However, the decrease in resistivity observed in the east may be related to the rise of saline waters at the level of a large fault zone detected further east by the VLF-EM method. The rest of the profiles appears relatively homogeneous, with low resistivity values at depth (5 to 10 $\Omega \cdot m$). Profiles 8, 9, 10, and 11 (Figures 11h, 11i, 11j, and 11k) were carried out southwest of the experimental site. According to drilling carried out in this area, the thickness of Quaternary conglomerates and alluvium is about 7 meters. These profiles show high resistivity only in the first 5 to 7 meters of the upper part ($\rho \geq 140 \Omega \cdot m$), corresponding to Quaternary conglomerates. At depth, the profiles appear homogeneous with low resistivity values (about 10 $\Omega \cdot m$), indicating that this area is not affected by saline water irrigation. Profiles P12, P13, and P14 (Figures 11l, 11m, and 11n) were conducted northeast of the surveyed area. These profiles reveal relatively homogeneous formations, except for a fracture zone oriented NW-SE and dipping to the SW. This fracture is located at a distance of 140 meters on profile P12, 220 meters on profile

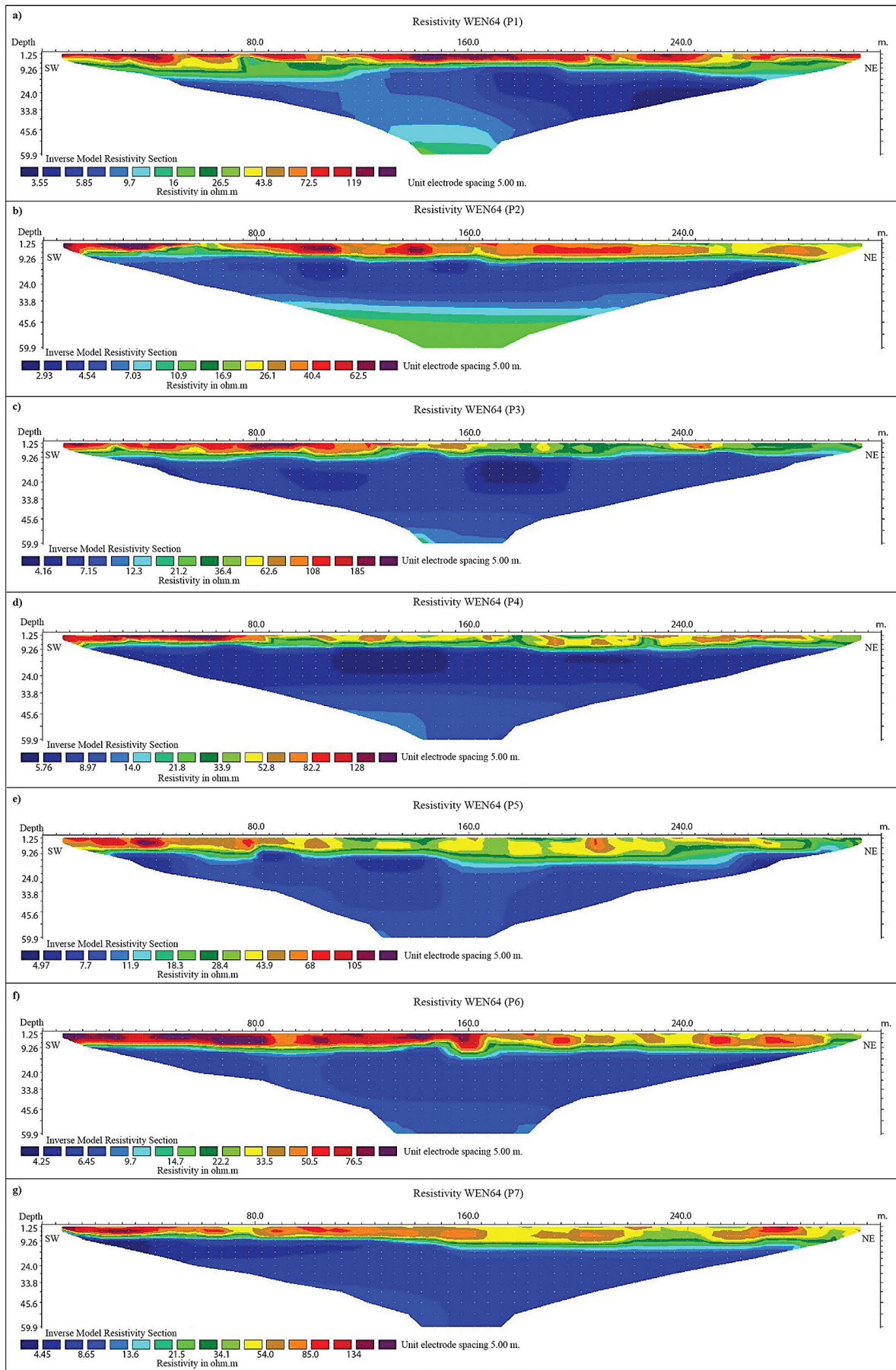


Figure 11. Electrical resistivity profiles conducted in the study area, with an inter-electrode spacing of 5 m

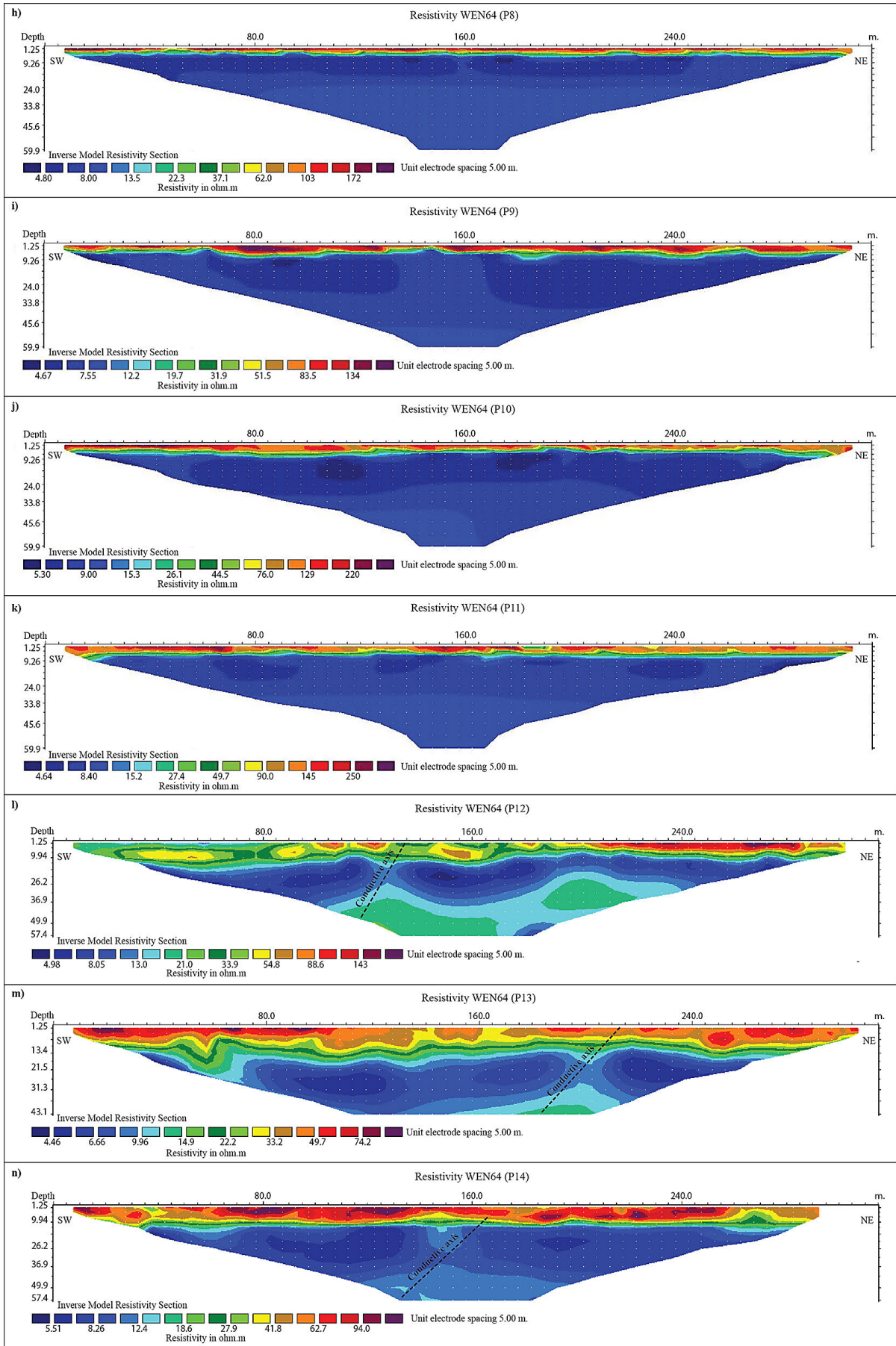


Figure 11. Cont.

P13, and 170 meters on profile P14. Moreover, this fracture zone coincides with the one detected by the VLF-EM method, thus confirming the correspondence between the results of the two geophysical methods.

Correlation of electromagnetic and electrical data

Figures 12, 13, and 14 present the interpretation of VLF-EM and ERT measurements performed on the Ain El Atti experimental station. Figure 11 illustrates the interpretation of the same geophysical methods applied in the southern part of the experimental station.

The Fraser data (Figures 12a, 13a, and 14a) reveal positive peaks located at distances of 700 m, 750 m, and 800 m, respectively. These anomalies suggest the presence of a conductive zone associated with a fracture zone. This interpretation is reinforced by the Karous-Hjelt pseudo-sections (Figures 12(b), 13(b), and 14(b)), which highlight a high concentration of electric currents indicating a marked geological discontinuity. The identified anomaly is characterized by a high current density and a dip toward the southwest. It is located approximately 700 m from the beginning of the profile and reaches a depth of 80 m. The NW-SE orientation of this structure suggests that it is a highly fractured zone, likely playing a key role in groundwater circulation.

The resistivity pseudo-sections in Figures 12(d) and 14(d) confirm the presence of this conductive anomaly by revealing a low-resistivity zone that coincides with a fracture structure extending over more than 50 m in depth. This structure is located at the same position detected in the Karous-Hjelt profiles, strengthening the correlation between the two methods.

The resistivity pseudo-sections in Figures 12(c), 13(c-d), and 14(c) show relative homogeneity of the formations at depth, with lateral and vertical variations in resistivity. These variations reflect the heterogeneous nature of the geological formations and their degree of water saturation. In the northeastern part of the profiles, saltwater irrigation has led to a significant reduction in surface resistivity (30 to 50 $\Omega\cdot\text{m}$) and an increase in the thickness of the affected layers. This observation suggests a progressive infiltration of saltwater into the superficial layers. In contrast, at the beginning of the profiles, where there is no irrigation, the surface resistivity is higher (120 to 140 $\Omega\cdot\text{m}$) and

lower at depth (5 to 10 $\Omega\cdot\text{m}$), which may indicate the presence of sandstones and marls.

Moving away from the irrigated area toward the southwest, the pseudo-section in Figure 13(c) shows a significant increase in surface resistivity (200 to 250 $\Omega\cdot\text{m}$), attributed to the presence of conglomerates, characterized by lower porosity and lower water retention capacity. However, at depth, the rest of the profile remains relatively homogeneous, suggesting continuity in the underlying formations.

The ERT and VLF-EM profiles (Figure 15) were performed in the southern part of the Ain El Atti experimental station. The goal of this investigation is to verify the continuity of the previously detected conductive anomaly and to compare the electromagnetic and electrical characteristics of this non-irrigated zone with those of the irrigated areas in the station.

The results from Fraser (Figure 11a) and Karous-Hjelt (Figure 11b) confirm the persistence of the conductive anomaly already identified in profiles conducted inside the experimental station. This anomaly is characterized by a high current density and a dip toward the southwest. It is located about 600 m away, reaching a depth of 80 m, while at the surface, it is manifested at around 750 m. This configuration suggests the presence of a fracture structure oriented NW-SE, playing a key role in groundwater circulation and facilitating the upward movement of saltwater to the surface.

The resistivity pseudo-sections in Figures 15(d) and 15(e), located in the eastern part of the study area, show a significant decrease in surface resistivity, with values ranging from 40 to 90 $\text{ohm}\cdot\text{m}$. In contrast, the pseudo-section in Figure 15(c), located to the west, shows higher values ranging from 130 to 220 $\text{ohm}\cdot\text{m}$. This decrease in resistivity in the east can be attributed to the upward movement of saltwater within the fracture zone identified at the center of pseudo-section P14. This phenomenon leads to a significant reduction in surface resistivity on profile P5, indicating a saturation of highly mineralized water. In contrast, profile P10, located further downstream and away from this fracture zone, does not seem to be affected by this upward saltwater movement, confirming a relatively homogeneous geological formation in this part of the site. This spatial variation in resistivity reflects the significant influence of fracture structures on the dynamics of groundwater and highlights the impact of local hydrogeological conditions on the electrical properties of the subsurface.

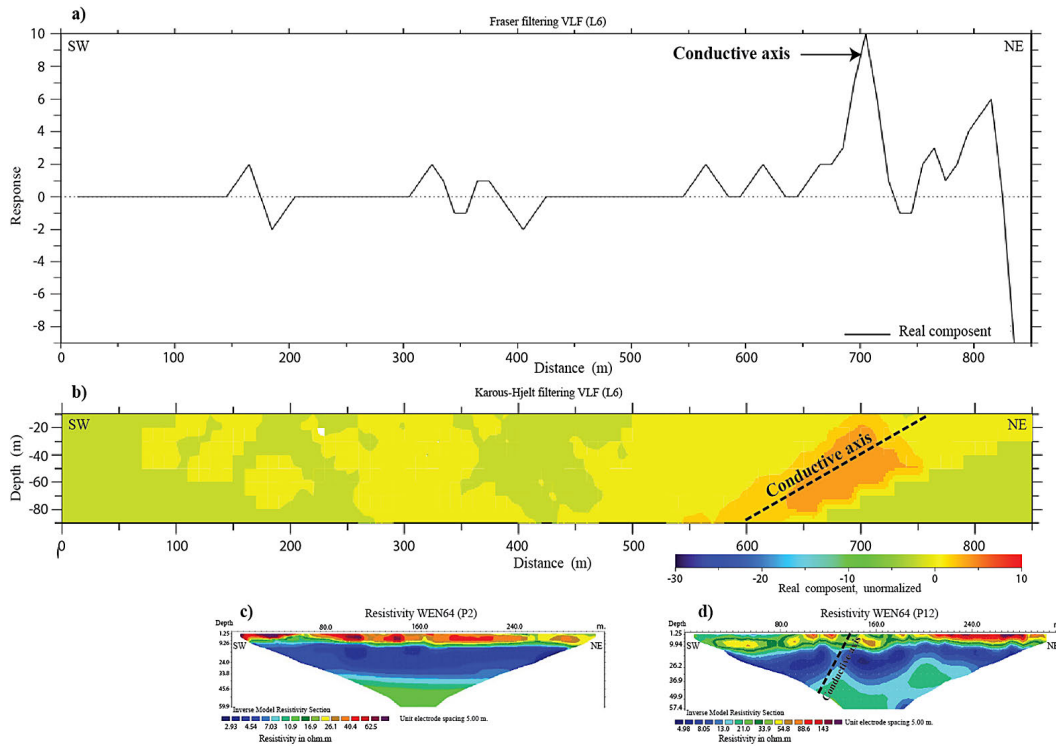


Figure 12. Interpretation of VLF-EM (L6) and ERT (P2 and P12) measurements. (a) Fraser filtering, (b) current density pseudo-section (Karous-Hjelt Filtering), (c-d) apparent resistivity pseudo-section

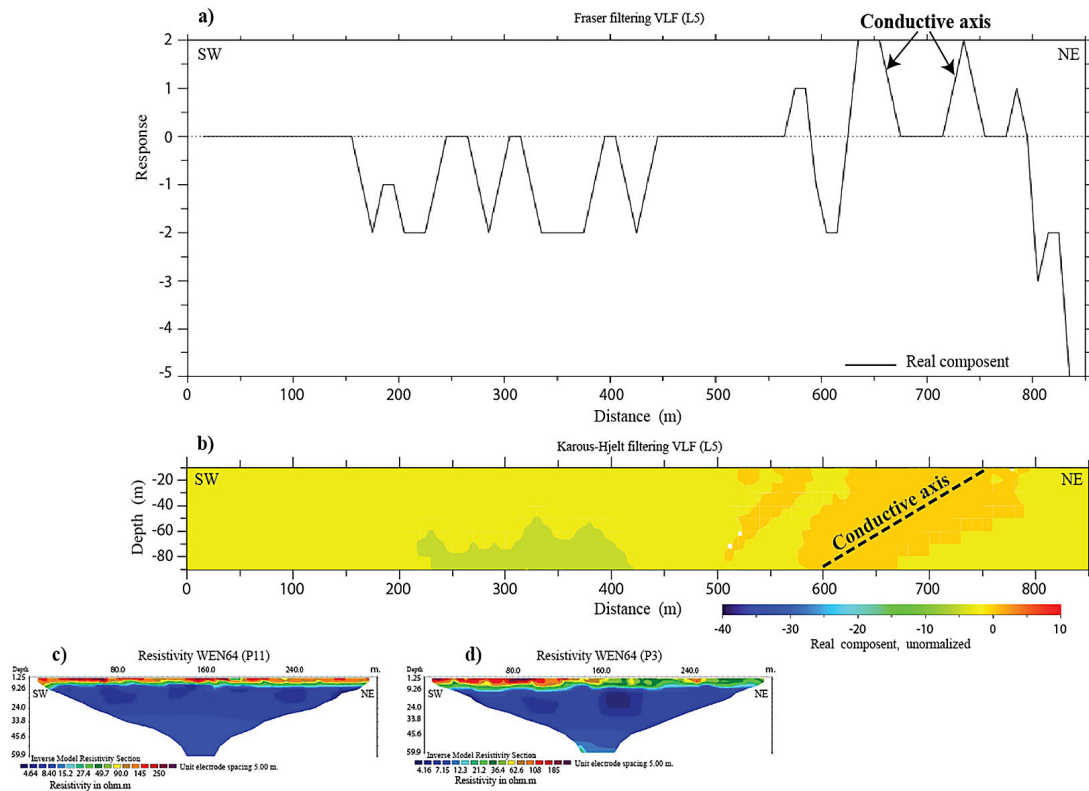


Figure 13. Interpretation of VLF-EM (L5) and ERT (P3 and P11) measurements. (a) Fraser filtering, (b) current density pseudo-section (Karous-Hjelt Filtering), (c-d) apparent resistivity pseudo-section

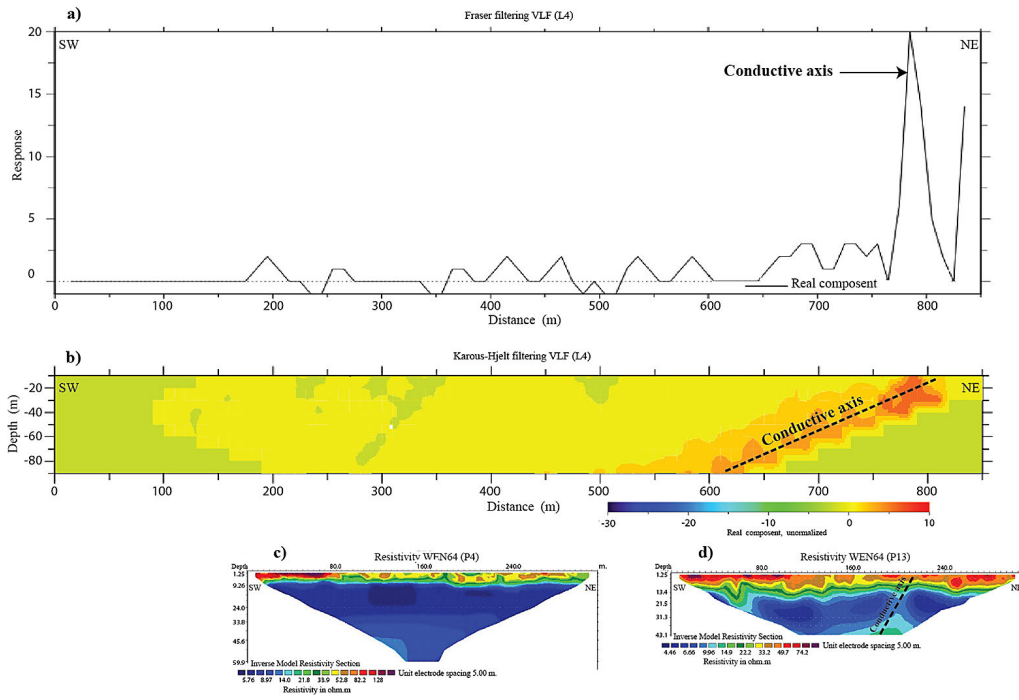


Figure 14. Interpretation of VLF-EM (L4) and ERT (P4 and P13) measurements. (a) Fraser filtering, (b) current density pseudo-section (Karous-Hjelt Filtering), (c-d) apparent resistivity pseudo-section

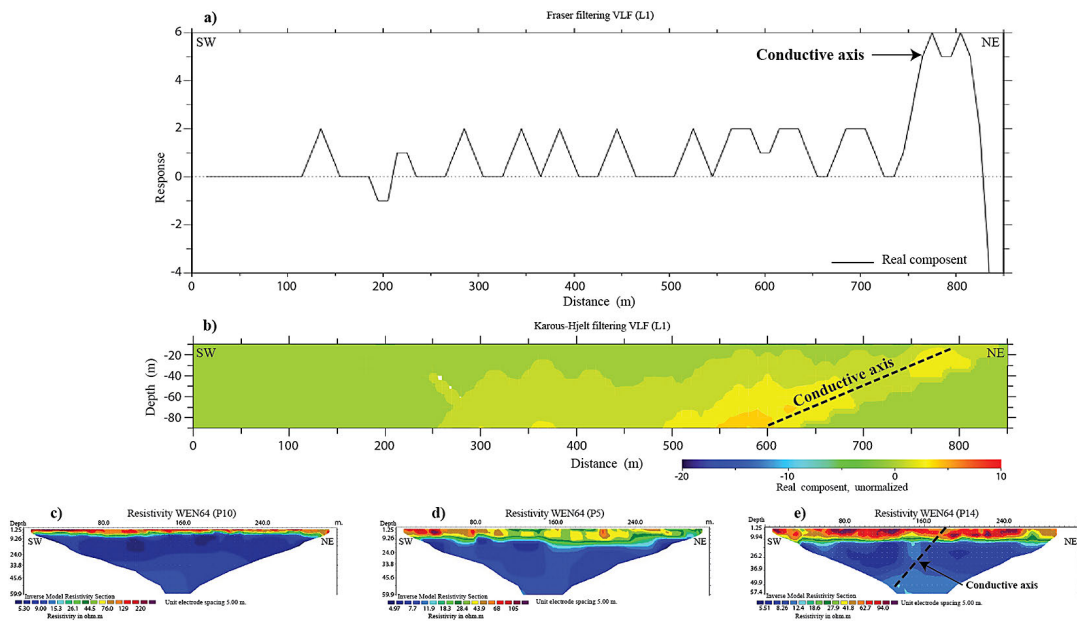


Figure 15. Interpretation of VLF-EM (L1) and ERT (P5, P10, and P14) measurements. (a) Fraser filtering, (b) current density pseudo-section (Karous-Hjelt Filtering), (c–d and e) apparent resistivity pseudo-section

CONCLUSIONS

The combined use of very low-frequency electromagnetic (VLF-EM) and ERT allowed us to effectively characterize the interactions between the local lithology and saline irrigation in the southern region of Errachidia, as well as identify the various

structural discontinuities. This approach led to new scientific results, revealing a previously unidentified NW-SE oriented fracture anomaly. This structure plays a key role in groundwater drainage and facilitates the upward movement of saline water to the surface, thus significantly influencing the spatial distribution of soil salinity.

One of the main findings of this study, through 3D Euler deconvolution analysis, is the identification of conductive anomalies attributed to gypsum marl formations at depths of up to 80 meters. These anomalies are aligned in a NW-SE direction, parallel to the fault identified in the SW part, which had not been fully understood in previous studies.

This research fills an important gap by demonstrating the influence of geological discontinuities, such as fractures, on the movement of saline water and soil salinization. The identification of the specific role of these fractures in groundwater dynamics adds a new dimension to the understanding of soil degradation in arid regions.

The study opens new perspectives for future research. Additional geophysical profiles in the northern part of the area would allow for an assessment of the continuity of the identified fracture and provide a better understanding of the regional lithology. Such research would also contribute to improving water management strategies and reducing groundwater contamination from underlying gypsum formations.

REFERENCES

- Ait Bahammou, Y., Benamara, A., Ammar, A., & Dakir, I. (2019). Fracture zones detection for groundwater exploration integrating Resistivity Profiling and Very Low Frequency electromagnetic methods (Errachidia basin, Morocco). *Contributions to Geophysics and Geodesy*, 49(2), 181–194. <https://doi.org/10.2478/congeo-2019-0009>
- Ait Bahammou, Y., Benamara, A., Ammar, A., Hritta, D., Dakir, I., & Bouikbane, H. (2021). Application of vertical electrical sounding resistivity technique to explore groundwater in the Errachidia basin, Morocco. *Groundwater for Sustainable Development* 15(10), 100648. <https://doi.org/10.1016/j.gsd.2021.100648>
- Ammar, A. I., & Kruse, S. E. (2016). Resistivity soundings and VLF profiles for siting groundwater wells in a fractured basement aquifer in the Arabian Shield, Saudi Arabia. *Journal of African Earth Sciences*, 116, 56–67. <https://doi.org/10.1016/j.jafrearsci.2015.12.020>
- Ammar, B. (2007). *Geochemical and isotopic study of the main aquifers of the Cretaceous Basin of Errachidia and the Tafilalet plain*. Thesis, Doc. Uni. Med V Agdal, Rabat, 134. (in French). https://www.researchgate.net/publication/277114719_Etude_geochimique_et_isotopique_des_principaux_aquiferes_du_bassin_Cretace_d'Errachidia_et_de_la_plaine_de_Tafilalet
- Ben-said, E., Boukdir, A., Mahboub, A., Younsi, A., El Moquaddam, K., Alili, L., & Zitouni, A. (2017). Contribution of statistics to the study of interactions between the jurassic aquatic watertable and the Hassan Addakhil Dam (Errachidia). *American Journal of Innovative Research and Applied Sciences*. 476–486 (in French). https://www.researchgate.net/publication/329196998_apport_de_la_statistique_a_l'etude_des_interactions_entre_la_nappe_jurassique_et_le_barrage_hassan_addakhil_errachidia
- Benson, A. K., Payne, K. L., & Stubben, M. A. (1997). Mapping groundwater contamination using dc resistivity and VLF geophysical methods—A case study. *Geophysics*, 62(1), 80–86.
- Bouzekraoui, M., Saadi, M., Essalhi, M., Karaoui, B., Hilali, M., Jayadi, S., & Bahaj, T. (2023). Extensional tectonics, structural architecture modeling and geodynamic evolution in the Cretaceous Tinghir-Errachidia-Boudenib basin (Pre-African Trough, Morocco). *J. Afr. Earth Sci.* 203, 104957 <https://doi.org/10.1016/j.jafrearsci.2023.104957>
- Chamayou, J., & Ruhard, J. P. (1977). *Pre-African trough to the east of Siroua: the Ouarzazate and Errachidia (Ksar-es-Souk)-Boudenib Basins*. Water Resources of Morocco, Atlas and South-Atlas Domains (in French).
- Chiara C., Sabrina B., & Cesare C. (2019) Comparison of laboratory and field electrical resistivity measurements of a gypsum rock for mining prospection applications. *International Journal of Mining Science and Technology*, 29(6), 841–849 <https://doi.org/10.1016/j.ijmst.2019.09.002>
- Chidiebere C. A., Chibuikwe A., Philip N. O., Anthony C. (2023) Integrated electrical resistivity methods for evaluation of fracture terrain groundwater potentials, case study of indurated shale of Lower Benue trough, Southeastern Nigeria. *Groundwater for Sustainable Development*, 23, 101014. <https://doi.org/10.1016/j.gsd.2023.101014>
- Choubert, G. (1920–1945). Essay on the paleogeography of Moroccan Mesocretacea. *Jubilee Volume, Moroccan Society of Natural Sciences, 1920–1945*, 307–329 (in French).
- Choubert, G., & Faure-Muret A. (1962). Evolution of Moroccan Atlas domain since the Paleozoic times. In: Durand-Delga M. (Ed.): Memory book P. Fallot, Mém. h. ser. Soc. Géol. France, Paris, 1 447–527 (in French). <http://pascal-francis.inist.fr/vibad/index.php?action=getRecordDetail&idt=19271547>
- Chouteau, M. (2001). Electrical, electromagnetic and seismic methods. lecture notes, polytechnic school, 158.
- Cooper, G. R. J. (2004). Euler deconvolution applied to potential field gradients. *Exploration Geophysics*,

- 35, 165–170. <https://doi.org/10.1071/EG04165>
15. Dakir, I., Benamara, A., Aassoumi, H., Ouallali, A., & Ait Bahammou, Y. (2020). Hydrogeophysics Exploration Approximately Ain Al Atti (Region of Southeast Erfoud Morocco). *Current Research in Geoscience*, 10(1), 16-26. <https://doi.org/10.3844/ajgsp.2020.16.26>
 16. Dakir, I., Benamara, A., Ouallali, A., & Ait Bahammou, Y. (2021). Application of electrical resistivity and electromagnetic methods to explore mineralized veins (copper and barite) in tinejda area (southeastern morocco). *Italian Journal of Engineering Geology and Environment 1*, 19–29. <https://doi.org/10.4408/IJEGE.2021-01.O-02>
 17. DRHGRZ (Regional Directorate of Hydraulics for the Guir-Rheris-Ziz basin) (2007). Hydrogeological synthesis study of cretaceous Errachidia basin. Report, 44. (in French). <https://www.raddo.org/Organismes/Agence-du-bassin-hydraulique-de-Guir-Ziz-Rheris-Maroc>
 18. Ebrahimi, A., Sundararajan, N., & Ramesh Babu, V. (2019). A comparative study for the source depth estimation of very low frequency electromagnetic (VLF-EM) signals. *J. Appl. Geophys.* 162, 174–183. <https://doi.org/10.1016/j.jappgeo.2019.01.007>
 19. Eze C. L., Mamah L. I., & Israel-Cookey C. (2004). Very low frequency electromagnetic (VLF-EM) response from a lead sulphide lode in the Abakaliki lead/zinc field, Nigeria. *International Journal of Applied Earth Observation and Geoinformation*, 5(2), 159–163. <https://doi.org/10.1016/j.jag.2004.01.004>
 20. Fraser, D. C. (1969). Contouring of VLF-EM data. *Geophysics*, 34, 958–967. <https://doi.org/10.1190/1.1440065>
 21. Gürer, A., Bayrak, M., & Gürer, Ö. F. (2009). A VLF survey using € current gathering phenomena for tracing buried faults of Fethiye–Burdur Fault Zone, Turkey. *J. Appl. Geophys.* 68(3), 437–447. <http://dx.doi.org/10.1016/j.jappgeo.2009.03.011>
 22. Hollard, H., Choubert, G., Bronner, G., Marchand, J., & Sougy, J. (1985). Geological map of Morocco scale 1/1000000. Notes Mem. Serv. Geol. Maroc. 260.
 23. Horo, d., Pal S.K., Singh S., Srivastava S. (2020) Combined self potential, electrical resistivity tomography, and induced polarisation for mapping of gold prospective zones over a part of Babaikundi-Birgoan Axis, North sighbhum Mobile belt, India. *Exploration Geophysics*, 51(5), 507–522.
 24. Karous, M., & Hjelt S. E. (1983). Linear filtering of VLF dip-angle measurements. *Geophysical Prospecting*, 31(5), 782–794. <https://doi.org/10.1111/j.1365-2478.1983.tb01085.x>
 25. Kaya, M. A., Özürlan, G., & Şengül, E. (2007). Delineation of soil and groundwater contamination using geophysical methods at a waste disposal site in Çanakkale, Turkey. *Environmental Monitoring and Assessment*, 135, 1–3, 441–446. <http://dx.doi.org/10.1007/s10661-007-9662-x>
 26. Kumar, S., Kumar Pal, S., & Guha, A. (2020). Very low frequency electromagnetic (VLF-EM) study over Wajrakarur kimberlite Pipe 6 in Eastern Dharwar Craton, India. *J. Earth Syst. Sci.* 129,102. <https://doi.org/10.1007/s12040-020-1367-3>
 27. Loke, M. H. (2004). Tutorial: 2-D and 3-D *Electrical Imaging Surveys*. https://www.researchgate.net/publication/264739285_Tutorial_2-D_and_3D_Electrical_Imaging_Surveys
 28. Loke, M. H., & Barker, R. D. (1996a). Rapid least-squares inversion of apparent resistivity pseudosections by a quasi-Newton method. *Geophysical Prospecting*, 44(1), 131–152. <https://doi.org/10.1111/j.1365-2478.1996.tb00142.x>
 29. Margat, J., (1977). Hydrogeological study of the quaternary basin of Tafilalet. *Water Resources of Morocco*, 310–380 (in French).
 30. Mushayandebvu, M. F., Van Driel, P., Reid, A. B., & Fairhead, J. D. (2001). Magnetic source parameters of two-dimensional structures using extended Euler deconvolution. *Geophysics* 66, 814–823. <https://doi.org/10.1190/1.1444971>
 31. Nabighian, M. N., & Hansen, R. O. (2001). Unification of Euler and Werner deconvolution in three dimensions via the generalized Hilbert transform. *Geophysics* 66, 1805–1810. <https://doi.org/10.1190/1.1487122>
 32. Olenchenko, V., & Osipova, P. (2022). Electrical Resistivity Tomography of Alluvial Deposits during Prospecting for Placer Gold. *Russian Geology and Geophysics* 63(1), 98–108. <https://doi.org/10.2113/RGG20204203>
 33. Pšsteka, R., & Kušnirák, D. (2020). *Role of Euler deconvolution in near surface gravity and magnetic applications*. In: Advances in Modeling and Interpretation in near Surface Geophysics. Springer, 223–262. http://dx.doi.org/10.1007/978-3-030-28909-6_9
 34. Reid, A. B., Allsop, J. M., Granser, H., Millett, A. J., & Somerton, I.W. (1990). Magnetic interpretation in three dimensions using Euler deconvolution. *Geophysics*, 55, 80–91. <https://doi.org/10.1190/1.1442774>
 35. Reid, A. B., Ebbing, J., & Webb, S. J. (2014). Avoidable Euler Errors - the use and abuse of Euler deconvolution applied to potential fields: avoidable Euler Errors. *Geophys. Prospect.* 62, 1162–1168. <https://doi.org/10.1111/1365-2478.12119>
 36. Saydam A. S., (198). Very low frequency electromagnetic interpretation using tilt angle and ellipticity measurements. *Geophysics*, 46, 11, 1594–1605. <https://doi.org/10.1190/1.1441166>
 37. Seaton, W. J., & Burbey, T. J. (2002). Evaluation

- of two-dimensional resistivity methods in a fractured crystalline-rock terrane. *Journal of Applied Geophysics*, 51, 21–41. [https://doi.org/10.1016/S09269851\(02\)00212-4](https://doi.org/10.1016/S09269851(02)00212-4)
38. Sharma, S., & Verma, G. K. (2015). Inversion of Electrical Resistivity Data: A Review. *International Journal of Computer and Systems Engineering*, 9(4) 400–406. https://scholar.google.com/scholar?q=Sharma,+S.,+Verma,+G.K.,+2015.+Inversion+of+Electrical+Resistivity+Data:+A+Review,+9.&hl=fr&as_sdt=0&as_vis=1&oi=scholar
39. Sharma, S. P., Biswas, A., & Baranwal, V.C. (2014). *Very low-frequency electromagnetic method: a shallow subsurface investigation technique for geophysical applications*. In: Sengupta, D. (Ed.), *Recent Trends in Modelling of Environmental Contaminants*. Springer India, New Delhi, pp. 119–141. https://doi.org/10.1007/978-81-322-1783-1_5
40. Sungkono, Santosa B.J., Bahri, A.S., Santos, F.M., & Iswahyudi, A. (2017). Application of noise-assisted multivariate empirical mode decomposition in VLF-EM data to identify underground river. *Adv. Data Sci. Adapt. Data Anal.* 9(1), 1650011. <https://doi.org/10.1142/S2424922X1650011X>
41. Tarik, L., Benamara, A., Chaibi, M., Tarik, M., Hritta, D., & Bouhali, K. (2023). Application and comparison of very low frequency electromagnetic and electrical resistivity techniques to investigate a Karstic Region: A case study of EL Hajeb Municipality, Morocco. *Journal of Applied Geophysics*, 215, 105121. <https://doi.org/10.1016/j.jappgeo.2023.105121>
42. Thompson, D. T. (1982). EULDPH: A new technique for making computer-assisted depth estimates from magnetic data. *Geophysics* 47, 31–37. <https://doi.org/10.1190/1.1441278>